ACS APPLIED MATERIALS & INTERFACES

Research Article

www.acsami.org

Simultaneous Improvement in Short Circuit Current, Open Circuit Voltage, and Fill Factor of Polymer Solar Cells through Ternary Strategy

Qiaoshi An,[†] Fujun Zhang,*[,†] Lingliang Li,[†] Jian Wang,[†] Qianqian Sun,[†] Jian Zhang,[‡] Weihua Tang,[§] and Zhenbo Deng[†]

[†]Key Laboratory of Luminescence and Optical Information, Ministry of Education, Beijing Jiaotong University, Beijing 100044, China

[‡]School of Materials Science and Engineering, Guilin University of Electronic Technology, Guilin, Guangxi 541004, China

[§]Key Laboratory of Soft Chemistry and Functional Materials, Ministry of Education, Nanjing University of Science and Technology, Nanjing, Jiangsu 210094, China

Supporting Information

ABSTRACT: We present a smart strategy to simultaneously increase the short circuit current (J_{sc}), the open circuit voltage (V_{oc}), and the fill factor (FF) of polymer solar cells (PSCs). A two-dimensional conjugated small molecule photovoltaic material (SMPV1), as the second electron donor, was doped into the blend system of poly(3-hexylthiophene) (P3HT) and [6,6]-phenyl-C71-butyric acid methyl ($PC_{71}BM$) to form ternary PSCs. The ternary PSCs with 5 wt % SMPV1 doping ratio in donors achieve 4.06% champion power conversion efficiency (PCE), corresponding to about 21.2% enhancement compared with the 3.35% PCE of P3HT:$PC_{71}BM$-based PSCs. The underlying mechanism on performance improvement of ternary PSCs can be summarized as (i) harvesting more photons in the longer wavelength region to increase J_{sc}; (ii) obtaining the lower mixed highest occupied molecular orbital (HOMO) energy level by incorporating SMPV1 to increase V_{oc}; (iii) forming the better charge carrier transport channels through the cascade energy level structure and optimizing phase separation of donor/acceptor materials to increase J_{sc} and FF.

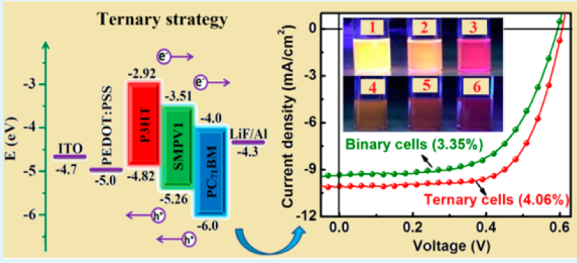

KEYWORDS: *polymer solar cells, ternary strategy, energy transfer, charge carrier transfer, energy level*

INTRODUCTION

Bulk heterojunction polymer solar cells (PSCs), as a promising photovoltaic technology, can be fabricated by solution processing and roll-to-roll manufacturing techniques with advantages of the better exciton dissociation efficiency and charge carrier transport due to the bicontinuous interpenetrating network in the active layers.[1−4] In recent years, PSCs have achieved a considerable progress in power conversion efficiency (PCE) that has exceeded 10% with various strategies.[5−7] It is generally believed that the PCE of PSCs is proportional to the product of short circuit current (J_{sc}), open circuit voltage (V_{oc}), and fill factor (FF).[8,9] In order to improve the PCE, many effective strategies have been carried out to increase the J_{sc}, V_{oc}, and FF (three key photovoltaic parameters) by developing novel narrow bandgap material and adapting tandem device structure or active layer treatment methods.[10−13] For instance, design and synthesis of narrow bandgap donor materials can harvest more photons from the solar light for J_{sc} improvement.[14−16] The tandem structure solar cells stacking two or more subcells can increase either the J_{sc} or V_{oc} for the subcells in parallel or series, while the intricate production process is a serious challenge for large-area fabrication.[17−19] The surface morphology, phase separation, and crystallinity of active layers can be optimized by incorporating an additive or employing proper annealing treatment for the J_{sc} and FF improvement.[20−23] Up to now, fewer strategies can simultaneously improve the three key photovoltaic parameters for the performance improvement of PSCs.[24]

It was recently shown that the ternary strategy is expected to play an important role in achieving high performance PSCs, which inherit the major benefit of incorporating multiple organic materials in tandem cells while retaining the simple cell fabrication technology.[25−30] Ameri et al. reported that the J_{sc} can be improved from 8.6 to 12 mA/cm^2 by doping a low bandgap material into the system of poly(3-hexylthiophene) (P3HT) and [6,6]-phenyl-C61-butyric acid methyl (PCBM), resulting in the PCE increasing from 3.1% to 4%.[31] Thompson et al. demonstrated that the V_{oc} can be gradually increased by only changing the doping weight ratios of two donors or two acceptors in ternary PSCs.[32−34] Chen and co-workers realized

Received: November 25, 2014
Accepted: January 27, 2015
Published: January 27, 2015

DOI: 10.1021/acsami.5b00308
ACS Appl. Mater. Interfaces 2015, 7, 3691−3698

the FF improvement from 40.6% to 54.3% by employing P3HT as an additive to adjust the morphology of the active layer.[35] It is reasonable to believe that the three key photovoltaic parameters of PSCs can be simultaneously optimized through a well-designed ternary strategy.

In the ternary strategy, the active layers with the polymer/polymer/fullerene system generally have a strong tendency to undergo enthalpy-driven phase separation, which results in serious phase separation with domain sizes in the micrometer range.[36] Ruderer et al. reported that the ideal scale of the phase separation in the active layer should be approximately equal to exciton diffusion length (~10 nm), which is a crucial factor to affect exciton dissociation and charge carrier transport.[37] The ternary strategies based on the polymer/polymer/fullerene system are less effective than the polymer/small molecule/fullerene system due to the large scale of the phase separation. Recently, Liu et al. reported a high efficient two-dimensional conjugated small molecule photovoltaic material (SMPV1) which has excellent solubility in organic solvents and a high absorption coefficient in the longer wavelength range.[38] There is a larger absorption spectral complementary between P3HT and SMPV1, which provides the opportunity to fabricate high efficiency ternary PSCs based on P3HT and SMPV1 as the electron donors. In this research, the small molecule material SMPV1, as the second electron donor, was mixed with P3HT and [6,6]-phenyl-C71-butyric acid methyl ($PC_{71}BM$) to fabricate ternary PSCs. The PCE values of PSCs were improved from 3.35% to 4.06% for the ternary cells with 5 wt % SMPV1 doping ratio in donors, which is attributed to a substantial improvement J_{sc} and FF as well as a slight V_{oc} increase.

EXPERIMENTAL SECTION

The patterned indium tin oxide (ITO) glass coated substrates (sheet resistance 15 Ω/□) were cleaned consecutively in ultrasonic baths containing acetone, detergent, deionized water, and ethanol, respectively. The cleaned ITO substrates were blow-dried by high pure nitrogen gas and then treated by UV−ozone for 10 min in order to further increase the work function of the ITO substrates. The poly(3,4-ethylenedioxythiophene):poly(styrenesulfonicacid) (PEDOT:PSS) (purchased from H.C. Starck co. Ltd.) thin films were fabricated on the cleaned ITO substrates by the spin-coating method at 5000 rounds per minute (RPM) for 40 s and then annealed at 150 °C for 10 min in an air environment. The electron donor materials P3HT and SMPV1 and electron acceptor materials $PC_{71}BM$ were purchased from Luminescence Technology Corp. The SMPV1 doping weight ratios are 0, 2.5, 5.0, 7.5, and 15 wt % in electron donors (P3HT and SMPV1), and the weight ratio of donors to acceptor was kept constant as 1:1. The mixed materials ($P3HT_{1-x}$:$SMPV1_x$:$PCBM_1$) were dissolved in 1,2-dichlorobenzene to fabricate 40 mg/mL blend solutions; the subscript represents SMPV1 doping ratio in donors, x = 0, 2.5, 5, 7.5, and 15 wt %, respectively. The blend solutions were spin-coated on PEDOT:PSS films at 900 rpm for 20 s in a high purity nitrogen-filled glovebox to fabricate the active layers. The thickness of the active layers is ~300 nm, which is measured by Ambios Technology XP-2 stylus Profiler. After that, the active layers were dried in a covered Petri dish for 1 h (without annealing treatment on the active layer). The combined cathode of LiF/Al (0.9 nm/100 nm) film was deposited on the active layer by thermal evaporation under 10^{-4} Pa, and the thickness was monitored by a quartz crystal microbalance. The active area is about 3.8 mm^2, defined by the vertical overlap of ITO anode and Al cathode. The schematic configuration of the PSCs and the chemical structures of electron donor and acceptor materials are shown in Figure 1.

The ultraviolet−visible (UV−vis) absorption spectra of films were obtained using a Shimadzu UV-3101 PC spectrometer. Ultraviolet photoemission spectroscopy (UPS) was measured by an ultrahigh vacuum system (10^{-9} Pa) with a hemispherical electron analyzer, a twin anode X-ray gun, and a He discharge lamp. Photoluminescence (PL) spectra of films were measured by a PerkinElmer LS-55 spectrophotometer. Time-resolved transient photoluminescence (TRTPL) spectra were obtained using a FluoroCube-01-NL and FluoroCub-NL from Jobin Yvon. The fabrication parameters of the above films for absorption, PL, TRTPL spectra, and UPS measurements are described in the Supporting Information. The current density−voltage (J−V) curves of all PSCs were measured in an air environment using a Keithley 2400 source meter. AM 1.5G irradiation at 100 mW/cm^2 was provided by an ABET Sun 2000 solar simulator. The external quantum efficiency (EQE) spectra of PSCs was measured by a Zolix Solar Cell Scan 100. The morphology of the blend films with different SMPV1 doping ratios in donors was investigated by atomic force microscopy (AFM) using a multimode Nanoscope IIIa operated in tapping mode. X-ray diffraction (XRD) patterns of blend films were collected using a Bruker D8 Advance X-ray diffractometer.

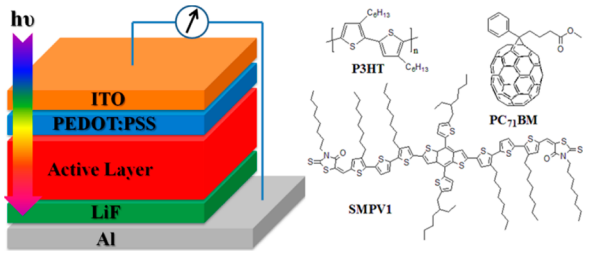

Figure 1. Schematic configuration of PSCs and the chemical structures of electron donor and acceptor materials.

RESULTS AND DISCUSSION

A series of PSCs with $P3HT_{1-x}$:$SMPV1_x$:$PC_{71}BM_1$ as the active layers was fabricated under the same conditions to investigate the effect of SMPV1 doping ratios in donors on the performance of PSCs (x = 0, 2.5, 5, 7.5, 15 wt %). The J−V curves and EQE spectra of all PSCs were measured under the same conditions and are shown in Figure 2. According to the J−V curves and EQE spectra of all PSCs, the key photovoltaic parameters of PSCs are summarized in Table 1. The champion PCE of 4.06% was obtained from the ternary PSCs with 5 wt % SMPV1 doping ratio in donors as the active layer, resulting from the simultaneous enhancement in J_{sc} (10.06 vs 9.32 mA/cm^2), V_{oc} (0.61 vs 0.59 V), and FF (66.3% vs 60.4%) compared with the control PSCs based on P3HT:$PC_{71}BM$ as the active layers. More than two hundred PSCs were fabricated from different batches to further confirm the effect of SPMV1 doping ratios in donors on the performance of PSCs; the typical J−V curves of the optimized ternary PSCs with 5 wt % SMPV1 doping ratio are shown in Figure S1, Supporting Information, and the key photovoltaic parameters are listed in Table S1 (Supporting Information).The average J_{sc}, V_{oc}, FF, and PCE values of ternary PSCs with 5 wt % SMPV1 doping ratio are 10.0 mA/cm^2, 0.607 V, 66.0%, and 4.0% based on seven cells prepared from different batches, respectively.

As described in Figure 2a, the J_{sc} of ternary PSCs is increased along with the increase of SMPV1 doping ratios (≤5 wt %) in donors and then decreased as SMPV1 doping ratios exceed 5 wt % in donors. The calculated J_{sc} values from the integration of the EQE spectra are close to the values obtained from J−V curves with the average error less than 2%, which indicates that the experimental results presented in this work are reliable. It is apparent that the EQE values of ternary PSCs are enhanced in the range from 600 to 700 nm along with the increase of SMPV1 doping ratios, as shown in Figure 2b. However, the

DOI: 10.1021/acsami.5b00308
ACS Appl. Mater. Interfaces 2015, 7, 3691−3698

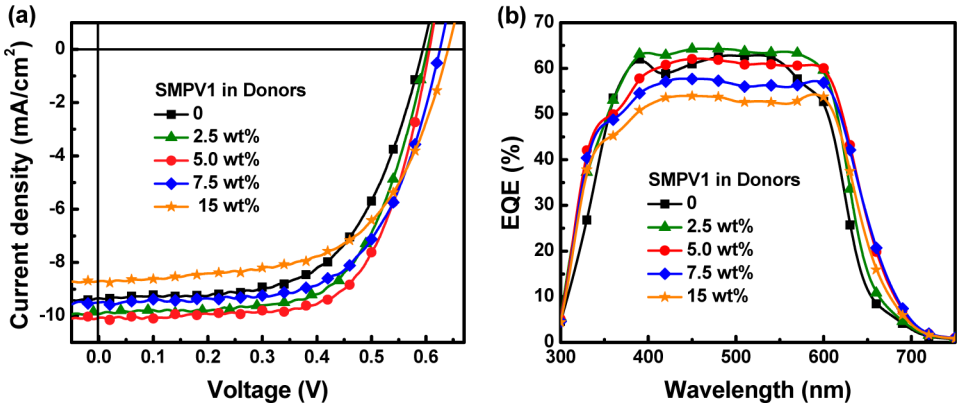

Figure 2. (a) $J-V$ curves of PSCs with different SMPV1 doping ratios in donors under AM 1.5 G illumination at 100 mW/cm^2; (b) EQE spectra of PSCs with different SMPV1 doping ratios in donors.

Table 1. Key Photovoltaic Parameters of PSCs with Different SMPV1 Doping Ratios

	PCE [%]							
SMPV1 [wt %]	best	average[a]	J_{sc} [mA/cm^2]	cal. J_{sc} [mA/cm^2]	V_{oc} [V]	FF [%]	R_S [Ω cm^2]	R_{SH} [Ω cm^2]
0	3.35	3.27	9.32	9.22	0.59	60.4	12.4	147
2.5	3.82	3.75	9.97	9.93	0.60	63.8	9.9	264
5.0	4.06	3.95	10.06	10.10	0.61	66.3	8.5	850
7.5	3.73	3.50	9.50	9.53	0.63	62.3	10.6	635
15	3.31	3.25	8.70	8.80	0.64	58.9	12.2	254

[a]Average PCE values are calculated on the basis of 30 PSCs prepared from different batches.

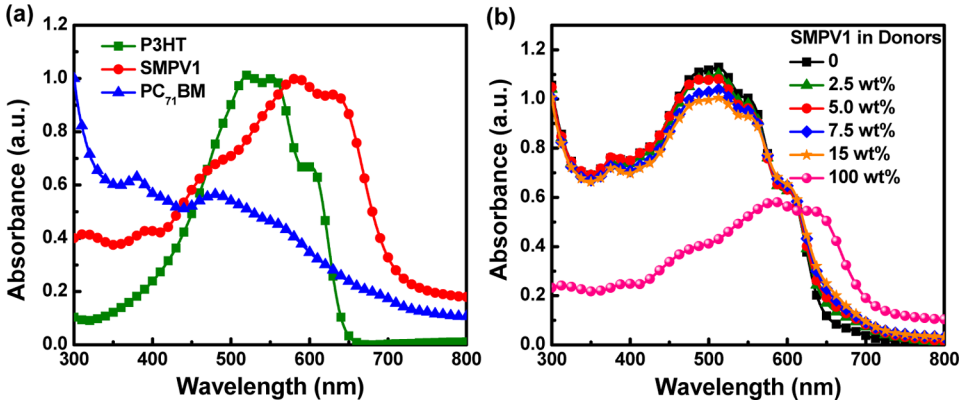

Figure 3. (a) Normalized UV−vis absorption spectra of neat P3HT, SMPV1, and $PC_{71}BM$ films; (b) absorption spectra of blend P3HT:SMPV1 films with different SMPV1 doping ratios and neat SPMV1 film.

EQE values of ternary PSCs begin to substantially decline in the range from 400 to 600 nm when the SMPV1 doping ratios are larger than 5 wt % in donors. The trade-off of EQE values at different spectral ranges results in the increase and then decrease of J_{sc} along with the increase of SMPV1 doping ratios. In order to clarify the effect of SMPV1 doping ratios in donors on J_{sc} and EQE spectra of ternary PSCs, the normalized and unnormalized absorption spectra of neat P3HT, SMPV1, and $PC_{71}BM$ films are shown in Figure 3a and Figure S2, Supporting Information, respectively. The absorption spectra of P3HT and $PC_{71}BM$ films show an apparent complementary absorption in the range from 300 to 600 nm. The SMPV1 has a broader absorption in the visible light range with a strong absorption from 500 to 700 nm, which may be considered as an excellent second electron donor material to harvest more photons in the longer wavelength region for P3HT:$PC_{71}BM$-based PSCs. The absorption spectra of ternary blend films with different SMPV1 doping ratios in donors are presented in Figure 3b. It is apparent that the absorption intensity of blend films is gradually enhanced in the spectral range from 600 to 700 nm along with the increase of SMPV1 doping ratios, which is beneficial to the J_{sc} improvement. However, the absorption intensity of the blend films is reduced in the range from 400 to 600 nm due to the relatively decreased P3HT content along with the increase of SMPV1 doping ratios, resulting in the decreased J_{sc} of PSCs with relatively high SMPV1 doping ratios (>5 wt %). The variation of J_{sc} can be well explained from the absorption spectra of blend films and EQE spectra of ternary PSCs with different SMPV1 doping ratios in donors.

Interestingly, the V_{oc} of ternary PSCs is monotonically increased along with the increase of SMPV1 doping ratio. As we know, the V_{oc} is mainly determined by the energy level difference between the highest occupied molecular orbital (HOMO) of electron donor and the lowest unoccupied

DOI: 10.1021/acsami.5b00308
ACS Appl. Mater. Interfaces 2015, 7, 3691−3698

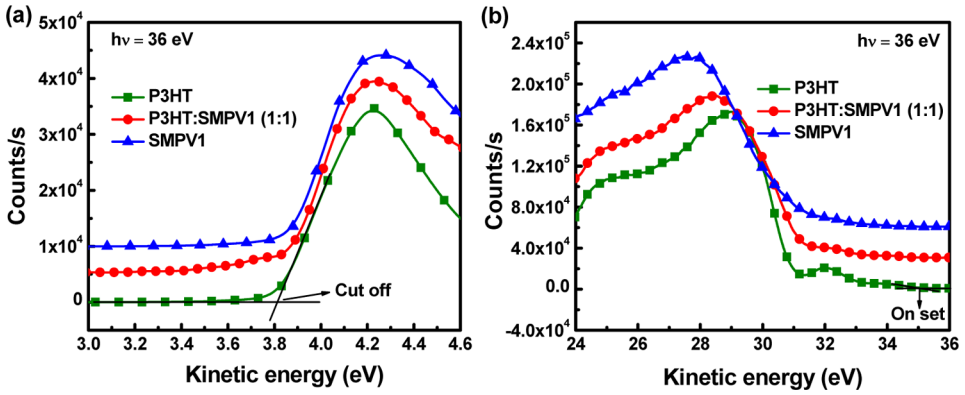

Figure 4. UPS spectra of the inelastic cutoff region (a) and HOMO region (b) of P3HT, P3HT:SMPV1 (1:1), and SMPV1 films (photon energy is 36 eV), measured in ultrahigh vacuum (10^{-9} Pa) conditions.

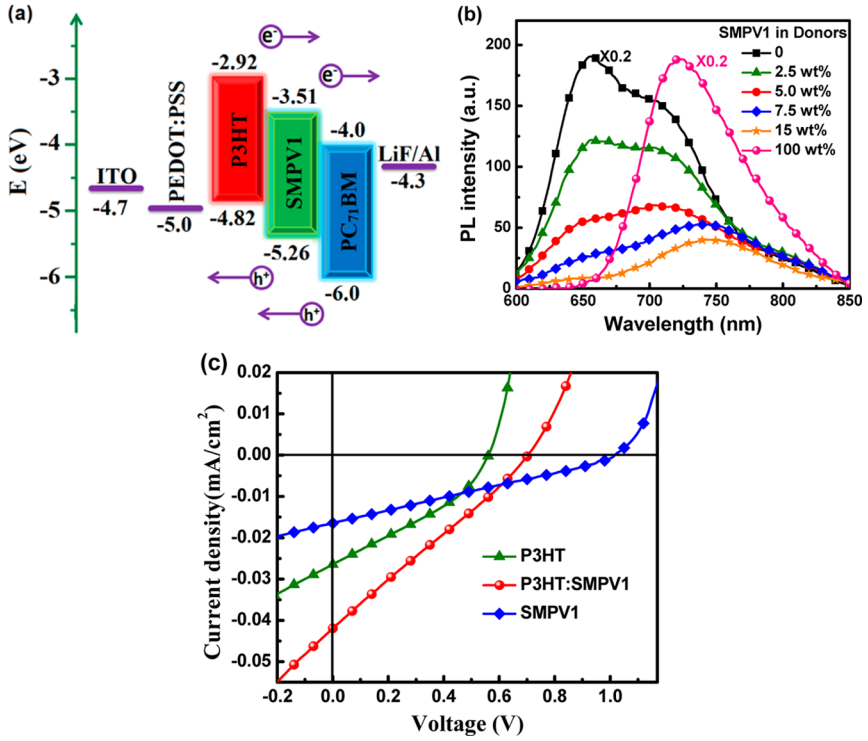

Figure 5. (a) Energy level diagram of ternary PSCs highlighting possible pathways for charge transfer and charge transport; (b) PL spectra of P3HT:SMPV1 films with different SMPV1 doping ratios under 490 nm wavelength light excitation; (c) $J-V$ curves of PSCs with P3HT, SMPV1, and P3HT:SMPV1 (1:1) as active layers (without $PC_{71}BM$) under AM 1.5 G illumination at 100 mW/cm^2.

molecular orbital (LUMO) of electron acceptor.[36,39,40] To clarify the effect of SMPV1 doping ratios on V_{oc} of ternary PSCs, the HOMO energy levels of P3HT, SMPV1, and P3HT:SMPV1 films were investigated by ultraviolet photoemission spectroscopy (UPS).[41,42] It is known that the HOMO energy level is calculated according to the following equation

$$E_{HOMO} = h\upsilon - (E_{onset} - E_{cutoff})$$

where $h\upsilon$ is the incident photon energy of 36 eV; E_{cutoff} is defined as the lowest kinetic energy of the measured electrons; E_{onset} is the HOMO energy onset, generally referred to as the high kinetic energy onset.[43,44] The E_{cutoff} and E_{onset} locations of P3HT, P3HT:SMPV1 (1:1), and SMPV1 films are marked in Figure 4a,b, respectively. According to Figure 4 and the above equation, the calculated HOMO energy levels (summarized in Table S2, Supporting Information) are −4.82 eV for P3HT, −4.97 eV for P3HT:SMPV1, and −5.26 for SMPV1. A series of PSCs with $P3HT_{0.5}$:$SMPV1_{0.5}$:$PC_{71}BM_1$ (0.5:0.5:1) as the active layers was fabricated to further demonstrate the effect of mixed HOMO levels of donors on V_{oc} of PSCs. The $J-V$ curves of PSCs under AM 1.5 G illumination at 100 mW/cm^2 are shown in Figure S3, Supporting Information, and the key parameters are listed in Table S3, Supporting Information. The V_{oc} of the PSCs is increased from 0.59 to 0.64 V for the cells with 15 wt % SMPV1 doping ratio and even to 0.73 V for the cells with 50 wt % SMPV1 doping ratio in donors. The monotonically increased V_{oc} of ternary PSCs can be understood from the decreased HOMO levels of P3HT:SMPV1 along with the increase of SMPV1 doping ratios.

According to the measured energy levels of P3HT and SMPV1 and reported energy levels of other materials, the energy level diagram of ternary PSCs is described in Figure

DOI: 10.1021/acsami.5b00308
ACS Appl. Mater. Interfaces 2015, 7, 3691−3698

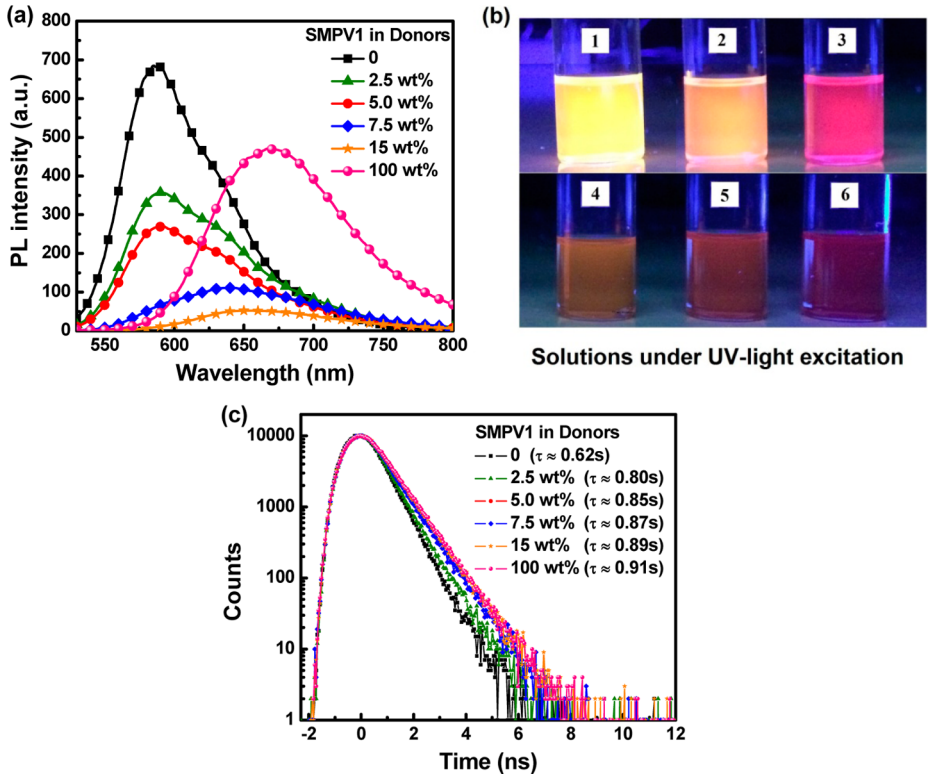

Figure 6. (a) PL spectra of P3HT:SMPV1 solutions with different SMPV1 doping ratios (excitation wavelength of 490 nm); (b) the photograph of different solutions (1-P3HT, 2-P3HT:SMPV1, 3-SMPV1, 4-P3HT:$PC_{71}BM$, 5-P3HT:SMPV1:$PC_{71}BM$, 6-SMPV1:$PC_{71}BM$) under UV-light excitation conditions; (c) TRTPL spectra of P3HT:SMPV1 solutions with different SMPV1 doping ratios (monitored at 670 nm).

5a.[28] The HOMO (−5.26 eV) and LUMO (−3.51 eV) energy levels of SMPV1 properly locate between the corresponding energy levels of P3HT and $PC_{71}BM$, respectively. The proper cascade energy level structure of P3HT, SMPV1, and $PC_{71}BM$ can provide several possible pathways for charge carrier transfer and transport among the electron donors and electron acceptor. The photogenerated excitons in P3HT or SMPV1 molecules can be directly dissociated into free charge carriers at the P3HT/$PC_{71}BM$ or SMPV1/$PC_{71}BM$ interfaces, respectively. The charge carrier transfer between P3HT and SMPV1 (electron transfer from P3HT to SMPV1 and hole transfer from SMPV1 to P3HT) may occur due to the suitable energy level alignment. As a consequence, charge carrier transfer is energetically allowed between P3HT and $PC_{71}BM$, between SMPV1 and $PC_{71}BM$, as well as between P3HT and SMPV1, which is beneficial to excitons dissociation, charge carrier transport, and collection.[45]

It is generally recognized that the FF strongly depends on the series resistances (R_S) and the shunt resistances (R_{SH}) of PSCs, which has tightly coupled relationships with exciton dissociation and charge carrier recombination in the active layer.[46−48] The optimized excitons dissociation and charge carrier transport should contribute to suppress charge carrier recombination, resulting in the increase of FF.[49] As seen from Table 1, it is apparent that the FF values of ternary PSCs are obviously higher than those of the control cells when SMPV1 doping ratio is lower than 7.5 wt % in donors. The optimized ternary PSCs (with 5% SMPV1 doping ratio) achieve the champion FF of 66.3% with the minimum R_S of 8.5 Ω cm^2 and the maximum R_{SH} of 850 Ω cm^2. To the best of our knowledge, the FF of 66.3% should be among the highest reported values for ternary PSCs.[50,51]

In order to further investigate the dynamic processes of charge carrier transfer or energy transfer between P3HT and SMPV1, PL spectra of P3HT:SMPV1 blend films with different SMPV1 doping ratios were measured under the excitation of 490 nm light and are shown in Figure 5b. It is apparent that neat P3HT and SMPV1films show strong emission peak at 660 and 720 nm, respectively. Generally, if energy transfer can occur from P3HT to SMPV1, one would expect a relatively increased SMPV1 emission intensity and decreased P3HT emission intensity for the blend P3HT:SMPV1 films along with increase of SMPV1 doping ratios, considering that the quantum yields of P3HT and SMPV1 are similar.[45,49] As seen from Figure 5b, both P3HT and SMPV1 emission intensities are substantially reduced along with the increase of SMPV1 doping ratios in donors due to charge carrier transfer between P3HT and SMPV1. Therefore, intermolecular energy transfer between P3HT and SMPV1 should be ignored. To further demonstrate the charge carrier transfer process between P3HT and SMPV1, a series of PSCs with P3HT, SMPV1, or P3HT:SMPV1 (1:1) as active layers were fabricated, respectively. The $J-V$ curves of three kinds of PSCs under AM 1.5 G illumination at 100 mW/cm^2 are shown in Figure 5c. The PSCs with P3HT:SMPV1(1:1) as the active layer display the largest J_{sc} compared with that of P3HT-based and SMPV1-based cells, which should be attributed to the effective charge carrier transfer between P3HT and SMPV1 supported by their cascade energy levels.

The PL spectra of P3HT:SMPV1 solutions with different SMPV1 doping ratios were measured under the 490 nm light excitation to further confirm the charge carrier transfer dynamic process between P3HT and SMPV1, as shown in Figure 6a. Expectedly, the PL spectra of blend solutions exhibit a similar

DOI: 10.1021/acsami.5b00308
ACS Appl. Mater. Interfaces 2015, 7, 3691−3698

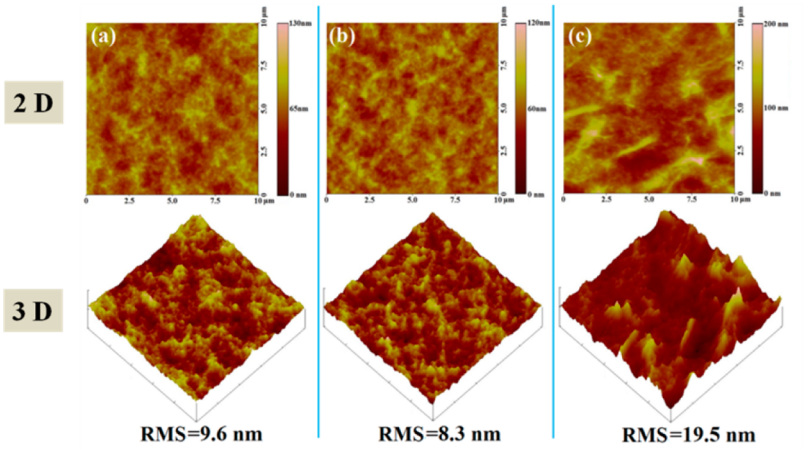

Figure 7. Two-dimensional (2D) and three-dimensional (3D) images of AFM morphology of (a) P3HT:$PC_{71}BM$ film as cast, (b) P3HT:SMPV1:$PC_{71}BM$ film with 5 wt % SMPV1 doping ratio in donors, and (c) P3HT:SMPV1:$PC_{71}BM$ film with 15 wt % SMPV1 doping ratio in donors.

varying tendency compared with the PL spectra of blend films. The PL spectral changes of blend solutions can be further confirmed from the relative solutions emission color under UV-light excitation conditions, as shown in Figure 6b. Meanwhile, PL emission intensity of P3HT:SMPV1 blend solutions can be markedly quenched by doping a small amount of $PC_{71}BM$ into blend solutions. Time-resolved transient photoluminescence (TRTPL) is a convenient tool to investigate the energy or charge transfer between different molecules. The TRTPL spectra of P3HT:SMPV1 solutions with different SMPV1 doping ratios were measured by monitoring 670 nm emission under the light excitation of 460 nm pulse NanoLED source. As shown in Figure 5c, the emission lifetime of 670 nm for neat P3HT solution is ~0.62 ns and gradually increased to ~0.89 ns for the blend P3HT:SMPV1 solution with 15 wt % SMPV1 doping ratio in donors. The emission lifetime of 670 nm for neat SMPV1 solution (~0.91 ns) is slightly longer than that for neat P3HT and blend P3HT:SMPV1 solutions, indicating that the energy transfer between P3HT and SMPV1 molecules can be absent or negligible.[52,53] The similar lifetime change trend is also observed from the TRTPL spectra for monitoring emission peak at 700 nm. The TRTPL spectra of blend solutions with different SMPV1 doping ratios were measured by monitoring 700 nm emission and are shown in Figure S4, Supporting Information, and the emission lifetime values of 670 and 700 nm are summarized in Table S4, Supporting Information. The decreased emission intensity of P3HT and SMPV1 should be due to the charge transfer rather than the energy transfer between P3HT and SMPV1 according to the PL spectra and TRTPL spectra of the blend solutions with different SMPV1 doping ratios.

To further illustrate the effect of SMPV1 doping ratios on the performance of the PSCs, the surface morphology and phase images of blend films were investigated by atomic force microscopy (AFM). The films for AFM characterization were prepared under the same conditions compared with the active layers of PSCs. The morphology and phase images of blend films with different SMPV1 doping ratios are shown in Figures S5 and S6, Supporting Information. Here, the morphology and phase images of P3HT:$PC_{71}BM$, $P3HT_{0.95}$:$SMPV1_{0.5}$:$PC_{71}BM_1$, and $P3HT_{0.85}$:$SMPV1_{0.15}$:$PC_{71}BM_1$ blend films are shown in Figure 7. The statistical average data root-mean-square (RMS) roughness of blend films are 9.6, 8.3, and 19.5 nm along with the increase of SMPV1 doping ratios in donors. The optimized surface morphology and phase separation of the ternary films with 5 wt % SMPV1 doping ratio may be beneficial to exciton dissociation, charge carrier transport, and collection, resulting in the improvement of J_{sc} and FF of PSCs. The RMS roughness of blend films is increased when SMPV1 doping ratios in donors are larger than 5 wt % due to SMPV1 molecular aggregation. The more and more obvious islands can be observed from AFM images when SMPV1 doping ratio exceeds 5 wt %, as shown in Figures S5 and S6, Supporting Information. The bicontinuous interpenetrating network of P3HT:$PC_{71}BM$ may be disturbed by relatively high SMPV1 doping ratios, which can be further demonstrated from the X-ray diffraction (XRD) pattern of blend films with different SMPV1 doping ratios and neat SMPV1 film.

Bearing in mind that the AFM investigation is only limited on the surface morphology and phase separation of films. In order to get better understandings of the effect of SMPV1 doping ratios on the performance of ternary PSCs, the molecular packing and crystalline structures of the ternary blend films are characterized by XRD, as shown in Figure 8. According to the XRD patterns, the key parameters are summarized in Table S5, Supporting Information. The control P3HT:$PC_{71}BM$ films exhibits a diffraction peak at $2\theta \approx 5.5°$ of ordered P3HT molecular arrangement corresponding to a d_{100}-spacing value of 16.05 Å.[39] The $2\theta \approx 5.5°$ diffraction peak intensity is decreased along with the increase of SMPV1 doping

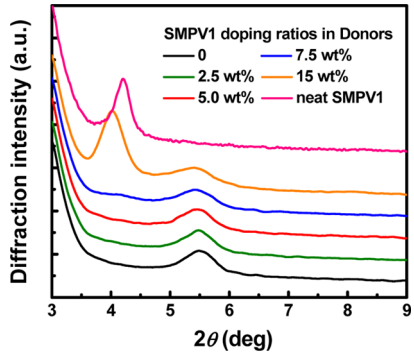

Figure 8. XRD patterns of $P3HT_{1-x}$:$SMPV1_x$:$PC_{71}BM_1$ films with different SMPV1 doping ratios in donors and neat SMPV1 film.

DOI: 10.1021/acsami.5b00308
ACS Appl. Mater. Interfaces 2015, 7, 3691−3698

ratios, which means that the ordered molecular arrangement of P3HT is disrupted by doping SMPV1.[54] A similar phenomenon has been already reported by Yu and co-workers in the system of P3HT:$PC_{71}BM$:SQ.[55] The neat SMPV1 films exhibit a strong diffraction peak at $2\theta \approx 4.2°$ corresponding to a d_{100}-spacing value of 20.97 Å. The blend films with 15 wt % SMPV1 doping ratio exhibit a strong diffraction peak at $2\theta \approx 4.0°$ corresponding to a d_{100}-spacing value of 21.94 Å, which should be attributed to the ordered arrangement of SMPV1 molecules.[38] The two diffraction peaks of blend films with 15 wt % SMPV1 doping ratio indicate that SMPV1 molecules aggregate in the blend films. The SMPV1 molecular aggregation in ternary films can disrupt the ordered molecular arrangement of P3HT, which may influence the exciton dissociation and charge carrier transport in the blend films.[36] Therefore, the decreased performance of ternary PSCs with relatively high SMPV1 doping ratios in donors can be reasonably understood due to the serious aggregation of SMPV1 and the disrupted P3HT molecular arrangement in blend films.

CONCLUSIONS

In conclusion, three key parameters of ternary PSCs-based P3HT:SMPV1:$PC_{71}BM$ as the active layers can be simultaneously increased when SMPV1 doping ratios in donors are lower than 5 wt %. The champion PCE of 4.06% is obtained on the basis of ternary PSCs with 5 wt % SMPV1 doping ratio in donors, corresponding to about 21.2% improvement compared with that of 3.35% PCE for P3HT:$PC_{71}BM$-based cells. The PCE improvement of ternary PSCs should be attributed to the better balance among photon harvesting, exciton dissociation, and charge carrier transport in blend films. The ternary strategy may open an effective way for high performance PSCs by retaining the major benefit of incorporating multiple organic materials in tandem cells and the simple fabrication technology of single bulk heterojunction PSCs.

ASSOCIATED CONTENT

Supporting Information

Typical $J-V$ curves of the ternary PSCs with 5 or 50 wt % SMPV1 doping ratio in donors; the parameters of energy levels of P3HT, SMPV1, and P3HT:SMPV1 with 1:1 weight ratio; TSTPL spectra of blend films with different SMPV1 doping ratios monitoring the emission peak at 700 nm; AFM surface morphology and phase 2D and 3D images of blend films with different SMPV1 doping ratios. This material is available free of charge via the Internet at http://pubs.acs.org.

AUTHOR INFORMATION

Corresponding Author

*Tel: 0086-10-51684908. E-mail: fjzhang@bjtu.edu.cn.

Notes

The authors declare no competing financial interest.

ACKNOWLEDGMENTS

This work was supported by Fundamental Research Funds for the Central Universities (2014JBZ017); National Natural Science Foundation of China (61377029, 21374120, and 61274063); National Natural Foundation of Distinguished Young Scholars of China (61125505); Beijing Natural Science Foundation (2122050) and Photoelectron Spectroscopy Endstation of the Beijing Synchrotron Radiation Facility.

REFERENCES

(1) Heeger, A. J. 25th Anniversary Article: Bulk Heterojunction Solar Cells: Understanding the Mechanism of Operation. *Adv. Mater.* **2014**, *26*, 10−27.
(2) Krebs, F. C.; Espinosa, N.; Hösel, M.; Søndergaard, R. R.; Jørgensen, M. 25th Anniversary Article: Rise to Power-OPV-Based Solar Parks. *Adv. Mater.* **2014**, *26*, 29−39.
(3) Bian, L.; Zhu, E.; Tang, J.; Tang, W.; Zhang, F. Recent Progress in the Design of Narrow Bandgap Conjugated Polymers for High-Efficiency Organic Solar Cells. *Prog. Polym. Sci.* **2012**, *37*, 1292−1331.
(4) Zhang, C.; Zhao, D.; Gu, D.; Kim, H.; Ling, T.; Wu, Y. K.; Guo, L. J. An Ultrathin, Smooth, and Low-Loss Al-Doped Ag Film and Its Application as a Transparent Electrode in Organic Photovoltaics. *Adv. Mater.* **2014**, *26*, 5696−5701.
(5) You, J.; Dou, L.; Yoshimura, K.; Kato, T.; Ohya, K.; Moriarty, T.; Emery, K.; Chen, C. C.; Gao, J.; Li, G.; Yang, Y. A Polymer Tandem Solar Cell with 10.6% Power Conversion Efficiency. *Nat. Commun.* **2013**, *4*, 1446−1455.
(6) You, J.; Chen, C. C.; Hong, Z.; Yoshimura, K.; Ohya, K.; Xu, R.; Ye, S.; Gao, J.; Li, G.; Yang, Y. 10.2% Power Conversion Efficiency Polymer Tandem Solar Cells Consisting of Two Identical Sub-Cells. *Adv. Mater.* **2013**, *25*, 3973−3978.
(7) Chen, C. C.; Chang, W. H.; Yoshimura, K.; Ohya, K.; You, J.; Gao, J.; Hong, Z.; Yang, Y. An Efficient Triple-Junction Polymer Solar Cell Having a Power Conversion Efficiency Exceeding 11%. *Adv. Mater.* **2014**, *26*, 5670−5677.
(8) Lin, Y.; Li, Y.; Zhan, X. Small Molecule Semiconductors for High-Efficiency Organic Photovoltaics. *Chem. Soc. Rev.* **2012**, *41*, 4245−4272.
(9) Zhang, F.; Xu, X.; Tang, W.; Zhang, J.; Zhuo, Z.; Wang, J.; Wang, J.; Xu, Z.; Wang, Y. Recent Development of the Inverted Configuration Organic Solar Cells. *Sol. Energy Mater. Sol. Cells* **2011**, *95*, 1785−1799.
(10) Guo, X.; Cui, C.; Zhang, M.; Huo, L.; Huang, Y.; Hou, J.; Li, Y. High Efficiency Polymer Solar Cells Based on Poly(3-hexylthiophene)/indene-C70 Bisadduct with Solvent Additive. *Energy Environ. Sci.* **2012**, *5*, 7943−7949.
(11) Wei, G.; Wang, S.; Sun, K.; Thompson, M. E.; Forrest, S. R. Solvent-Annealed Crystalline Squaraine: $PC_{70}BM$ (1:6) Solar Cells. *Adv. Energy Mater.* **2011**, *1*, 184−187.
(12) Ma, W.; Yang, C.; Gong, X.; Lee, K.; Heeger, A. J. Thermally Stable, Efficient Polymer Solar Cells with Nanoscale Control of the Interpenetrating Network Morphology. *Adv. Funct. Mater.* **2005**, *15*, 1617−1622.
(13) Zhao, D. W.; Liu, P.; Sun, X. W.; Tan, S. T.; Ke, L.; Kyaw, A. K. K. An Inverted Organic Solar Cell with an Ultrathin Ca Electron-Transporting Layer and MoO_3 Hole-Transporting Layer. *Appl. Phys. Lett.* **2009**, *95*, 153304.
(14) McNeill, C. R.; Abrusci, A.; Hwang, I.; Ruderer, M. A.; Muller-Buschbaum, P.; Greenham, N. C. Photophysics and Photocurrent Generation in Polythiophene/Polyfluorene Copolymer Blends. *Adv. Funct. Mater.* **2009**, *19*, 3103−3111.
(15) Hou, J. H.; Chen, H. Y.; Zhang, S. Q.; Chen, R. I.; Yang, Y.; Wu, Y.; Li, G. Synthesis of a Low Band Gap Polymer and Its Application in Highly Efficient Polymer Solar Cells. *J. Am. Chem. Soc.* **2009**, *131*, 15586−15587.
(16) Lu, L. Y.; Yu, L. P. Understanding Low Bandgap Polymer PTB7 and Optimizing Polymer Solar Cells Based on It. *Adv. Mater.* **2014**, *26*, 4413−4430.
(17) Ameri, T.; Khoram, P.; Min, J.; Brabec, C. J. Organic Ternary Solar Cells: A Review. *Adv. Mater.* **2013**, *25*, 4245−4266.
(18) Yang, L.; Zhou, H.; Price, S. C.; You, W. Parallel-Like Bulk Heterojunction Polymer Solar Cells. *J. Am. Chem. Soc.* **2012**, *134*, 5432−5435.
(19) Khlyabich, P. P.; Burkhart, B.; Rudenko, A. E.; Thompson, B. C. Optimization and Simplification of Polymer-Fullerene Solar Cells through Polymer and Active Layer Design. *Polymer* **2013**, *54*, 5267−5298.

DOI: 10.1021/acsami.5b00308
ACS Appl. Mater. Interfaces 2015, 7, 3691−3698

(20) Zhao, D. W.; Tan, S. T.; Ke, L.; Liu, P.; Kyaw, A. K. K.; Sun, X. W.; Lo, G. Q.; Kwong, D. L. Optimization of an Inverted Organic Solar Cell. *Sol. Energy Mater. Sol. Cells* **2010**, *94*, 985−991.
(21) Gholamkhass, B.; Servati, P. Solvent-Vapor Induced Morphology Reconstruction for Efficient PCDTBT Based Polymer Solar Cells. *Org. Electron.* **2013**, *14*, 2278−2283.
(22) Guo, X.; Zhou, N.; Lou, S. J.; Smith, J.; Tice, D. B.; Hennek, J. W.; Ortiz, R. P.; Navarrete, J. T. L.; Li, S.; Strzalka, J. Polymer Solar Cells with Enhanced Fill Factors. *Nat. Photonics* **2013**, *7*, 825−833.
(23) Xiao, Z.; Yuan, Y.; Yang, B.; VanDerslice, J.; Chen, J.; Dyck, O.; Duscher, G.; Huang, J. Universal Formation of Compositionally Graded Bulk Heterojunction for Efficiency Enhancement in Organic Photovoltaics. *Adv. Mater.* **2014**, *26*, 3068−3075.
(24) He, Z.; Zhong, C.; Huang, X.; Wong, W. Y.; Wu, H.; Chen, L.; Su, S.; Cao, Y. Simultaneous Enhancement of Open-Circuit Voltage, Short-Circuit Current Density, and Fill Factor in Polymer Solar Cells. *Adv. Mater.* **2011**, *23*, 4636−4643.
(25) Chen, M.; Li, M.; Wang, H.; Qu, S.; Zhao, X.; Xie, L.; Yang, S. Side-Chain Substitution of Poly(3-hexylthiophene) (P3HT) by PCBM via Postpolymerization: An Intramolecular Hybrid of Donor and Acceptor. *Polym. Chem.* **2013**, *4*, 550.
(26) Zhang, Y.; Basel, T. P.; Gautam, B. R.; Yang, X.; Mascaro, D. J.; Liu, F.; Vardeny, Z. V. Spin-Enhanced Organic Bulk Heterojunction Photovoltaic Solar Cells. *Nat. Commun.* **2012**, *3*, 1043.
(27) Kokil, A.; Poe, A. M.; Bae, Y.; Della Pelle, A. M.; Homnick, P. J.; Lahti, P. M.; Kumar, J.; Thayumanavan, S. Improved Performances in Polymer BHJ Solar Cells Through Frontier Orbital Tuning of Small Molecule Additives in Ternary Blends. *ACS Appl. Mater. Interfaces* **2014**, *6*, 9920−9924.
(28) Lessard, B. H.; Dang, J. D.; Grant, T. M.; Gao, D.; Seferos, D. S.; Bender, T. P. Bis(tri-*n*-hexylsilyl oxide) Silicon Phthalocyanine: A Unique Additive in Ternary Bulk Heterojunction Organic Photovoltaic Devices. *ACS Appl. Mater. Interfaces* **2014**, *6*, 15040−15051.
(29) An, Q.; Zhang, F.; Li, L.; Zhuo, Z.; Zhang, J.; Tang, W.; Teng, F. Enhanced Performance of Polymer Dolar Cells by Employing a Ternary Cascade Energy Structure. *Phys. Chem. Chem. Phys.* **2014**, *16*, 16103−16109.
(30) Ruderer, M. A.; Hinterstocker, M.; Müller-Buschbaum, P. Structure in Ternary Blend Systems for Organic Photovoltaics. *Synth. Met.* **2011**, *161*, 2001−2005.
(31) Ameri, T.; Min, J.; Li, N.; Machui, F.; Baran, D.; Forster, M.; Schottler, K. J.; Dolfen, D.; Scherf, U.; Brabec, C. J. Performance Enhancement of the P3HT/PCBM Solar Cells through NIR Sensitization Using a Small-Bandgap Polymer. *Adv. Energy Mater.* **2012**, *2*, 1198−1202.
(32) Khlyabich, P. P.; Burkhart, B.; Thompson, B. C. Efficient ternary Blend Bulk Heterojunction Solar Cells with Tunable Open-Circuit Voltage. *J. Am. Chem. Soc.* **2011**, *133*, 14534−14537.
(33) Khlyabich, P. P.; Burkhart, B.; Thompson, B. C. Compositional Dependence of the Open-Circuit Voltage in Ternary Blend Bulk Heterojunction Solar Cells Based on Two Donor Polymers. *J. Am. Chem. Soc.* **2012**, *134*, 9074−9077.
(34) Street, R. A.; Davies, D.; Khlyabich, P. P.; Burkhart, B.; Thompson, B. C. Origin of the Tunable Open-Circuit Voltage in Ternary Blend Bulk Heterojunction Organic Solar Cells. *J. Am. Chem. Soc.* **2013**, *135*, 986−989.
(35) Chang, S. Y.; Liao, H. C.; Shao, Y. T.; Sung, Y. M.; Hsu, S. H.; Ho, C. C.; Su, W. F.; Chen, Y. F. Enhancing the Efficiency of Low Bandgap Conducting Polymer Bulk Heterojunction Solar Cells Using P3HT as a Morphology Control Agent. *J. Mater. Chem. A* **2013**, *1*, 2447−2452.
(36) Cha, H.; Chung, D. S.; Bae, S. Y.; Lee, M. J.; An, T. K.; Hwang, J.; Kim, K. H.; Kim, Y. H.; Choi, D. H.; Park, C. E. Complementary Absorbing Star Shaped Small Molecules for the Preparation of Ternary Cascade Energy Structures in Organic Photovoltaic Cells. *Adv. Funct. Mater.* **2013**, *23*, 1556−1565.
(37) Ruderer, M. A.; Mueller-Buschbaum, P. Morphology of Polymer Based Bulk Heterojunction Films for Organic Photovoltaics. *Soft Mater.* **2011**, *7*, 5482−5493.
(38) Liu, Y.; Chen, C. C.; Hong, Z.; Gao, J.; Yang, Y. M.; Zhou, H.; Dou, L.; Li, G.; Yang, Y. Solution-Processed Small Molecule Solar Cells: Breaking the 10% Power Conversion Efficiency. *Sci. Rep.* **2013**, *3*, 3356−3363.
(39) Campoy-Quiles, M.; Kanai, Y.; El-Basaty, A.; Sakai, H.; Murata, H. Ternary Mixing: A Simple Method to Tailor The Morphology of Organic Solar Cells. *Org. Electron.* **2009**, *10*, 1120−1132.
(40) Li, H.; Zhang, Z. G.; Li, Y.; Wang, J. Tunable Open-Circuit Voltage in Ternary Organic Solar Cells. *Appl. Phys. Lett.* **2012**, *101*, 163302.
(41) Li, Z. H.; Wu, Z. H.; Mo, G.; Xing, X. Q.; Liu, P. A Small-Angle X-Ray Scattering Station at Beijing Synchrotron Radiation Facility. *Instrum. Sci. Technol.* **2014**, *42*, 128−141.
(42) Li, Z. H. A Program for SAXS Data Processing and Analysis. *Chin. Phys. C* **2013**, *37*, 1−6.
(43) Yang, T. B.; Wang, M.; Duan, C. H.; Hu, X. W.; Huang, L.; Peng, J. B.; Huang, F.; Gong, X. Inverted Polymer Solar Cells with 8.4% Efficiency by Conjugated Polyelectrolyte. *Energy Environ. Sci.* **2012**, *5*, 8208−8214.
(44) Zhang, F. J.; Vollmer, A.; Zhang, J.; Xu, Z.; Rabe, J. P.; Koch, N. Energy Level Alignment and Morphology of Interfaces Between Molecular and Polymeric Organic Semiconductors. *Org. Electron.* **2007**, *8*, 606−614.
(45) Koppe, M.; Egelhaaf, H.-J.; Dennler, G.; Scharber, M. C.; Brabec, C. J.; Schilinsky, P.; Hoth, C. N. Near IR Sensitization of Organic Bulk Heterojunction Solar Cells: Towards Optimization of the Spectral Response of Organic Solar Cells. *Adv. Funct. Mater.* **2010**, *20*, 338−346.
(46) Mauer, R.; Howard, I. A.; Laquai, F. Effect of Nongeminate Recombination on Fill Factor in Polythiophene/Methanofullerene Organic Solar Cells. *J. Phys. Chem. Lett.* **2010**, *1*, 3500−3505.
(47) Gupta, D.; Mukhopadhyay, S.; Narayan, K. S. Fill Factor in Organic Solar Cells. *Sol. Energy Mater. Sol. Cells* **2010**, *94*, 1309−1313.
(48) Qi, B.; Wang, J. Fill Factor in Organic Solar Cells. *Phys. Chem. Chem. Phys.* **2013**, *15*, 8972−8982.
(49) Lu, L. Y.; Xu, T.; Chen, W.; Landry, E. S.; Yui, L. P. Ternary Blend Polymer Solar Cells with Enhanced Power Conversion Efficiency. *Nat. Photonics* **2014**, *8*, 716−722.
(50) Ameri, T.; Heumüller, T.; Min, J.; Li, N.; Matt, G.; Scherf, U.; Brabec, C. J. IR Sensitization of an Indene-C60 Bisadduct (ICBA) in Ternary Organic Solar Cells. *Energy Environ. Sci.* **2013**, *6*, 1796−1801.
(51) Cheng, P.; Li, Y.; Zhan, X. Efficient Ternary Blend Polymer Solar Cells with Indene-C60 Bisadduct as an Electron-Cascade Acceptor. *Energy Environ. Sci.* **2014**, *7*, 2005−1011.
(52) Huang, J. S.; Goh, T.; Li, X. K.; Sfeir, M. Y.; Bielinski, E. A.; Tomasulo, S.; Lee, M. L.; Hazari, N.; Taylor, A. D. Polymer Bulk Heterojunction Solar Cells Employing Forster Resonance Energy Transfer. *Nat. Photonics* **2013**, *7*, 480−486.
(53) An, Q.; Zhang, F.; Li, L.; Wang, J.; Zhang, J.; Zhou, L.; Tang, W. Improved Efficiency of Bulk Heterojunction Polymer Solar Cells by Doping Low-Bandgap Small Molecules. *ACS Appl. Mater. Interfaces* **2014**, *6*, 6537−6544.
(54) Wan, X. J.; Liu, Y. S.; Wang, F.; Zhou, J. Y.; Long, G. K.; Chen, Y. S. Improved Efficiency of Solution Processed Small Molecules Organic Solar Cells Using Thermal Annealing. *Org. Electron.* **2013**, *14*, 1562−1569.
(55) Wang, H. Y.; Zheng, Y. F.; Zhang, L.; Yu, J. S. Effect of Two-Step Annealing on the Performance of Ternary Polymer Solar Cells Based on P3HT:$PC_{71}BM$:SQ. *Sol. Energy Mater. Sol. Cells* **2014**, *128*, 215−220.

DOI: 10.1021/acsami.5b00308
ACS Appl. Mater. Interfaces 2015, 7, 3691−3698